

Morphing Winglet Design for Aerodynamic Performance Optimization of the CRJ-700 Aircraft. Part 1 – Structural Design

Paul MEYRAN¹, Hugo PAIN¹, Ruxandra Mihaela BOTEZ^{*1}, Jeremy LALIBERTÉ²

*Corresponding author

¹Department of Systems Engineering, École de Technologie Supérieure,
1100 Notre Dame West, Montreal, Que., Canada, H3C-1K3,
ruxandra.botez@etsmtl.ca*

²Department of Mechanical and Aerospace Engineering, Carleton University,
Ottawa, Ont., Canada

DOI: 10.13111/2066-8201.2021.13.4.10

Received: 26 August 2021/ Accepted: 01 November/ Published: December 2021

Copyright © 2021. Published by INCAS. This is an “open access” article under the CC BY-NC-ND license (<http://creativecommons.org/licenses/by-nc-nd/4.0/>)

Abstract: *This study aims to design a morphing winglet structure for the CRJ-700 regional transport aircraft. The morphing technology is applied on winglets to demonstrate a significant increase of the aerodynamic performance of aircraft. From the aerodynamic data of the LARCASE Virtual Research Simulator VRESIM, the aerodynamic benefits in the cruising phase were obtained through a study on the ParaView software. The morphing winglet design was drawn using CATIA V5; this new concept included several structural components, as well as a simple and light mechanism allowing to orientate the winglet angles between 90° and -90° of inclination. The structural model was exported to HyperMesh structural analysis software. Maximum stresses were obtained, and the model demonstrated its resistance to maximum aerodynamic loads as well as load factors of -2G to 7G.*

Key Words: *Design, Morphing Winglet, Aerodynamics, Structure, Optimization*

1. INTRODUCTION

The current aviation industry faces major environmental challenges [1]. Indeed, the International Air Transport Association aims to achieve a “reduction in net aviation CO₂ emissions of 50% by 2050, relative to 2005 levels” [2].

To preserve a healthy environment for future generations, reducing fuel consumption is now undeniable. To make the aviation sector greener, the development of new technologies should be used, and morphing wing technology could be one of them.

To make transport planes more efficient, different methods exist to reduce fuel consumption, through improving aerodynamic performance.

Reducing the overall drag of the aircraft is today a major source of aerodynamic benefits. The vortices at the end of the wing, sources of a significant induced drag, could be minimized thanks to the use of winglets.

Today, the winglets represent an additional structure at the end of the wing and are not suitable for every flight condition as they are fixed and non-moving structures. As a result, the concept of a morphing winglet was developed.



Figure 1: Morphing winglet for the CRJ-700 aircraft

The overall objective of this paper is to propose a new concept of morphing winglet allowing the CRJ-700 regional transport aircraft to optimize its aerodynamic performance in cruise flight. To achieve this purpose, we will begin by identifying the winglet's inclinations that provide the best aerodynamic performance for the Bombardier CRJ-700 aircraft in cruise flight. Then, we will design a structure and mechanism for varying the orientation of the morphing winglet between -90° and 90° of inclination. After that, we will demonstrate that the designed morphing winglet structure will withstand the loads applied to it.

2. AERODYNAMIC ANALYSIS

The aerodynamic analysis carried out in this article is divided into two studies, the first emphasizing the optimal inclinations of the morphing winglet in the cruise phase and the second evaluating the aerodynamic loads applied to the winglet. We firstly analyzed the different winglet inclinations: -73° , -35° , 0° , 35° and 73° . All flight configurations considered an altitude of 30,000 ft and a Mach number of 0.8 because we focused our study on the cruise flight phase. A first series of winglet configurations considered a 0° angle of incidence, and a second series used a 4° angle of incidence. Based on a CFD study by Segui on the VRESIM of the LARCASE, we were able to visualize the pressure distribution over the entire CRJ-700 using the ParaView software [3]-[4].

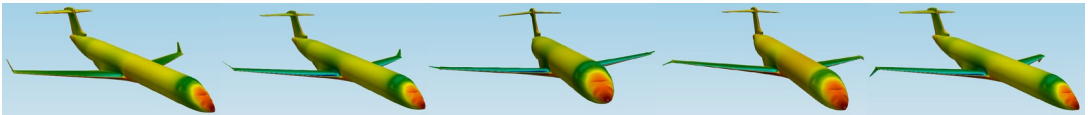


Figure 2: Morphing winglet simulations for a 0° angle of attack and different winglet inclinations

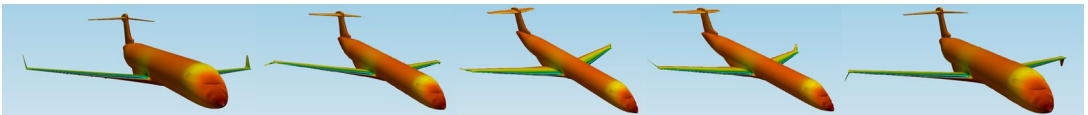


Figure 3: Morphing winglet simulations for a 4° angle of attack and different winglet inclinations

We calculated the lift and drag generated for these different winglet configurations. Thus, we could identify the best inclinations of the morphing winglet for angles of attack of 0° and 4° . The winglet inclination giving the greatest lift was the 0° inclination. Compared to the initial inclination of the winglet at $+73^\circ$, a lift improvement of 1.89% for a 4° angle of attack, and a lift improvement of 2.46% for a 0° angle of attack were obtained, as seen on Figure 4(a). We also noticed that a winglet in a negative orientation will develop greater lift than the winglet in positive (opposite) orientation.

The winglet inclination with the least drag is its 0° inclination for a 0° angle of attack and the

+73° for a 4° angle of attack. Compared to the initial inclination of the winglet at +73°, a decrease in drag of 1.45% for a 0° angle of attack was obtained when the winglet was at a 0° inclination. We obtained the best drag results when the angle of attack was 0° compared to when the angle of attack was 4°. In fact, during cruise, the airplanes fly at 0° incidence, and this is the configuration where the least drag is generated, which agrees with our results, as seen on Figure 4(b).

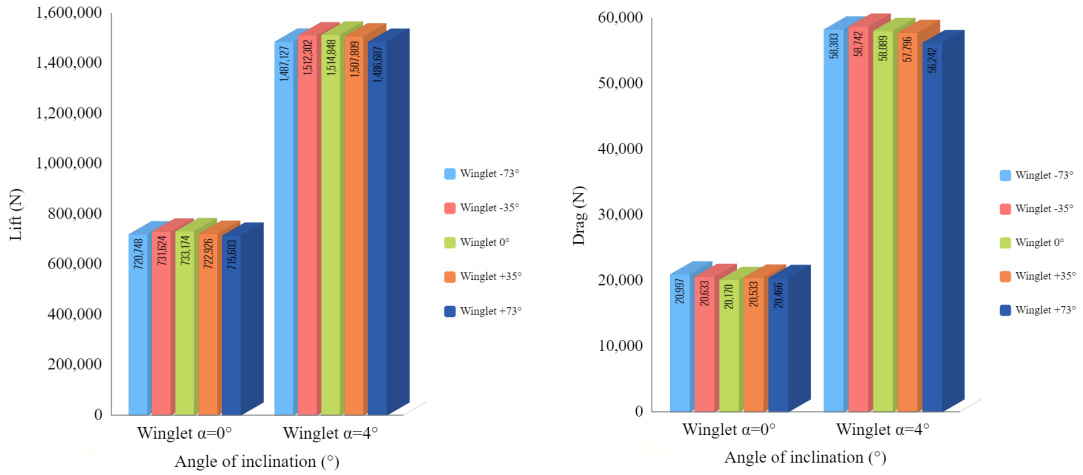


Figure 4: Lift (a) and drag (b) results for different morphing winglet configurations

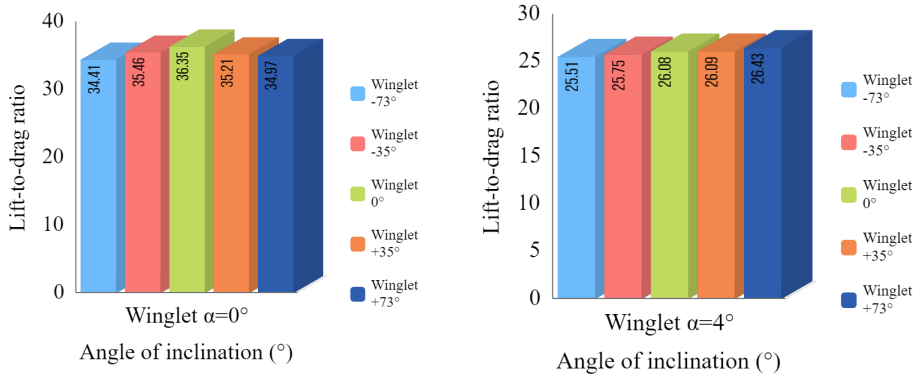


Figure 5: Lift-to-drag ratio results for different morphing winglet configurations

To complete this aerodynamic analysis, we calculated the lift-to-drag ratio for these different configurations. Thus, we could identify the best inclinations of the morphing winglet for angles of attack of 0° and 4°. For a 0° angle of attack, we noticed that a 0° inclination produced the highest lift-to-drag ratio. Compared to the initial inclination of the winglet at +73°, an increase in lift-to-drag ratio of 3.95% was obtained. For a 4° angle of attack, we noticed that a +73° winglet inclination produced the highest lift-to-drag ratio.

Therefore, in cruising conditions where the angle of attack is 0°, it will therefore be necessary to use a morphing winglet inclination around 0°. When the aircraft changes its flight altitude, it will therefore be necessary to use an inclination of the morphing winglet around +73°. To perform the analysis of aerodynamic loads, we secondly studied the evolution of pressures along the wing. To do it, we decided to make several successive cutting planes along the wing at relatively small distance intervals in order to achieve excellent analysis accuracy.

By making these different successive cutaways, we obtained the exact pressures to be applied to each airfoil from the wing root to the winglet tip.

Then, the aerodynamic forces along the wing were calculated from pressures. The distributions of these forces are obtained along the wing. We selected the maximum curve obtained for the lift and we neglected the drag curves.

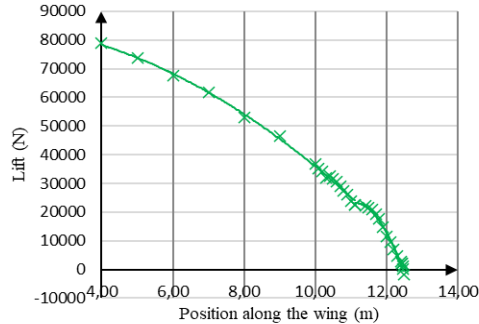


Figure 6: Evolution of maximum lift forces along the wing

We were able to calculate the maximum lift force from the root of the wing to the tip of the morphing winglet.

We also noted the maximum lift forces at the root and the pivot point of the morphing winglet. Indeed, we identified the point of lift drop located at 11 meters from the wing root as the point of rotation of the morphing winglet.

$$L_{winglet\ root} (x = 10) \approx 36\ 000\ N$$

$$L_{pivot\ point} (x = 11) \approx 25\ 000\ N$$

$$L_{winglet\ tip} (x = 12,5) \approx 0\ N$$

3. DESIGN OF THE MORPHING WINGLET

The design of the morphing winglet carried out in this article is divided into: 1) the design of the structure and 2) the design of the mechanism and the actuator. This research aims to design a morphing winglet that will perform 180° of inclination, including 90° upwards relative to the wing and 90° downwards relative to the wing. We set the morphing winglet inclination to 0° as the initial basis of this study.



Figure 7: NACA 20612 supercritical airfoil

The structure of the morphing winglet that we present in this paper is made up of spars, ribs, and skin.

All these elements were designed on CATIA V5 design software. A wing is a successive sequence of different airfoils defining the aerodynamic properties of the wing.

For the CRJ-700 aircraft, we found the NACA 20612 airfoil to best match the wing airfoil shape of the aircraft. This is a so-called supercritical airfoil because it is used for transonic speeds.

Aerodynamically speaking, in a supercritical airfoil, the separation of its boundary layer moves towards its trailing edge, thus improving the distance traveled along the wing airfoil in laminar flow.

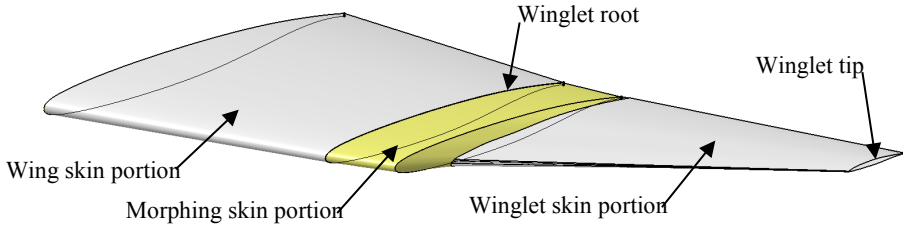


Figure 8: Morphing winglet skin characteristics

We have determined that the front spar will be positioned at 25% of the airfoil chord along the wing and winglet portions while the rear spar will be positioned at 75% of the chord. We have chosen to use C-sections for spars.

To complete the structural skeleton of the morphing winglet, we designed the ribs as sheet metal elements that will be attached to the spars and to the skin. We identified the front rib, the mid rib, and the rear rib.

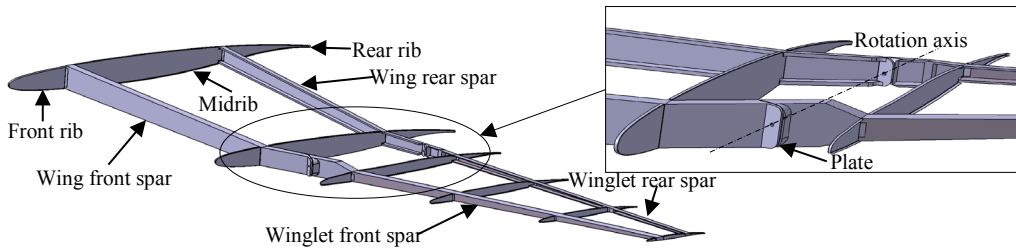


Figure 9: Morphing winglet internal structure characteristics

To design a mechanism that allows the morphing winglet structure to rotate, we modeled the pivot connection occurring between the wing and the winglet parts. The rotational motion between these two parts was integrated into the spars.

Therefore, we had two pivots to model, one taking place at the front spar and the other one at the rear spar.

To align the rotation centers of the front spars and the rear spars, we integrated plates to the spars, which will slide in rotation to allow the desired morphing winglet inclination. With this initial design of the morphing winglet structural skeleton, we can use any desired morphing winglet inclinations, ranging from -90° to $+90^\circ$.

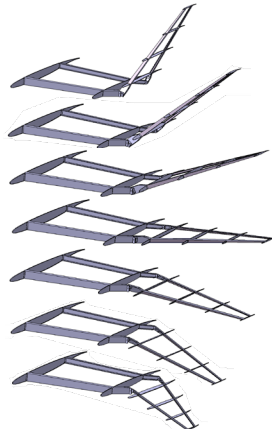


Figure 10: Morphing winglet structure variation of inclination

To allow the rotation of the morphing winglet, a pivot point was placed under the pivot connection of the winglet front spar at a distance R of the rotation axis. By moving this pivot point around its connection, the winglet front spar will rotate relative to the wing front spar.

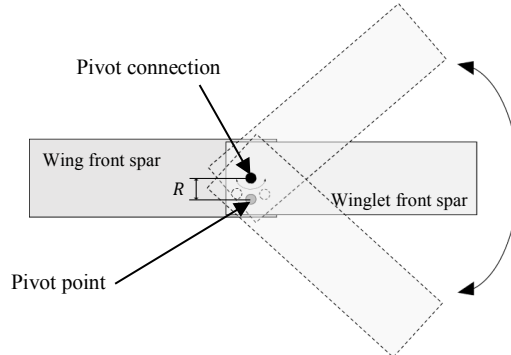


Figure 11: Pivot point modeling of the morphing winglet

Next, we therefore mechanically designed the pivot connection and the pivot point. To eliminate the friction linked to the rotation between the two parts, we used radial contact ball bearings. Knowing that it is the shaft that will turn, the inner ring of our bearings was mounted tight. Thus, we will prevent the lamination phenomenon from occurring. In addition, the rotating shaft is tightly mounted on the winglet front spar, so that, when the shaft rotated, the beam in question followed the same rotation as the shaft.

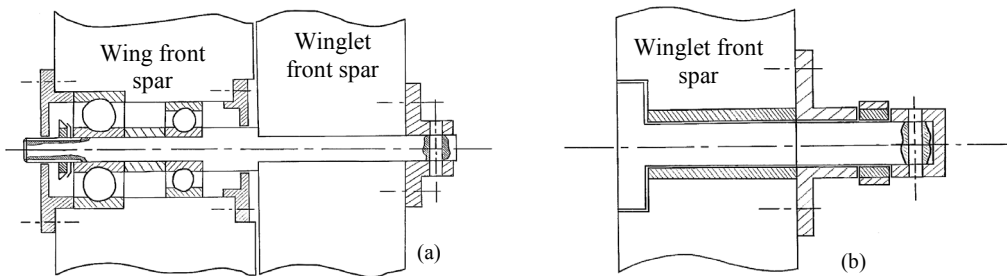


Figure 12: Industrial drawing of the pivot connection (a) and pivot point (b) for the morphing winglet

The assembly process of this pivot connection was ensured. The first bearing acting as an annular linear connection abuts against the shoulder of the shaft. Then, the spacer fixed the inner ring of the bearing. Then the second bearing acting as a point link was inserted on the shaft and abuts against the spacer for the inner ring, and against the shoulder of the bore for the outer ring. The inner race of this bearing was then secured by a lock nut using a lock washer type. Then, a lip seal secured the outer race of the bearing and provided a seal. Another lip seal was used on the other side to provide a seal. Finally, the mobile beam was inserted and fixed to the shaft with a fastening piece at the end of the shaft.

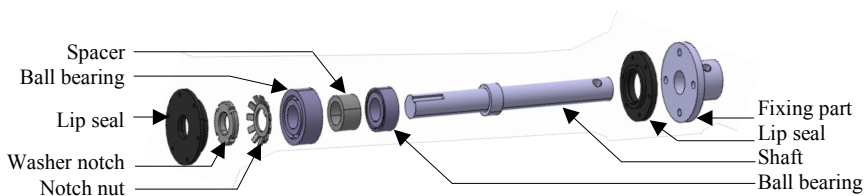


Figure 13: Design of the mechanical parts of the pivot connection

At the pivot point, we placed the actuation to rotate the morphing winglet. We used plain bearings to avoid friction between the rotating shaft and the bore of the beam, and the actuator. These plain bearings were mounted tightly on the bores. Only the front spar has a pivot point as we will only have one actuator that will move the morphing winglet. We mounted tightly the bushing on the bore. Next, we inserted the shaft from the left of the beam. We added a fixing part on the shaft, which was screwed onto the winglet front spar. It is used to position the actuator arm that rotates the morphing winglet. A plain bearing is placed in the hole in the actuator arm to reduce friction and wear on the actuator. Finally, the positioning of the actuator arm is fixed by a cap and a pin to block the actuator arm in translation along the shaft.

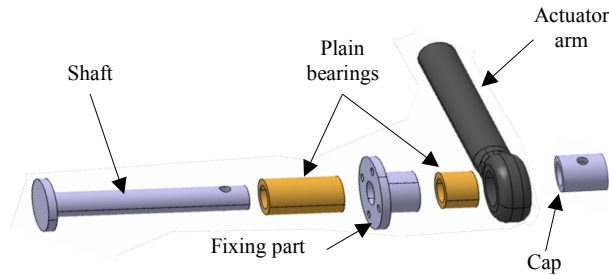


Figure 14: Design of the mechanical parts of the pivot point

The mechanisms for activating wing control surfaces often use hydraulic systems as actuators. However, the latter are bulky and heavy, this is the reason why the aviation is moving towards the electrification of these systems [5]. Smaller, lighter, more compact, and more reliable, today's electric actuators can support large loads. Aviation linear electromechanical actuators are using a DC motor, a reduction device, and a worm mechanism. The DC motor converts electrical energy (electric current) into mechanical energy (rotational speed). This rotational speed is adapted by a reduction box made up of gears to control the speed of the actuator stroke. Indeed, the screw and nut device convert a rotational movement into a translational movement. This movement will conduct the displacement of the morphing winglet.

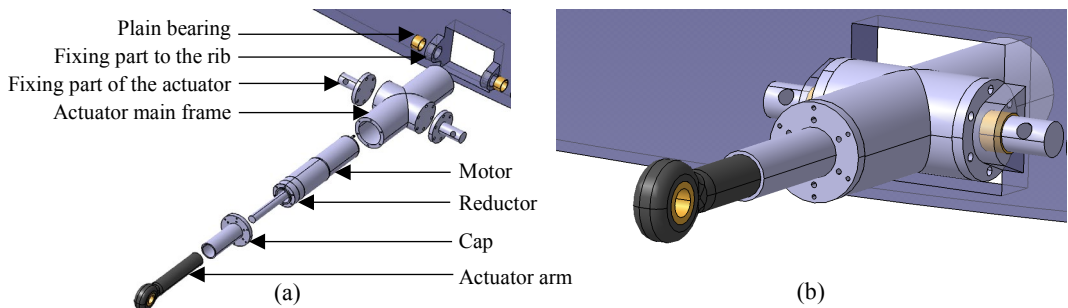


Figure 15: Mechanical parts design of the actuator (a) and actuator assembly on the rib (b)

To orientate the morphing winglet, the mechanism is always energized in order to keep the winglet in a desired inclination. As a safety measure, we designed a damper for our mechanism, so that the damper weakens the amplitude of shocks or vibrations that could occur in flight. Thus, the actuator would not be damaged. The shock absorber was added to the pivot point shaft, parallel to the actuator. We have chosen for a hydropneumatic shock absorber with spring which will dissipate the energy brought in by shocks or vibrations. The damper was attached to the root rib of the morphing winglet and to the back of its structure. Thus, the axial forces that it will undergo will be transmitted to the rib directly and the shock absorber will have an axial reaction force to resist the shocks.

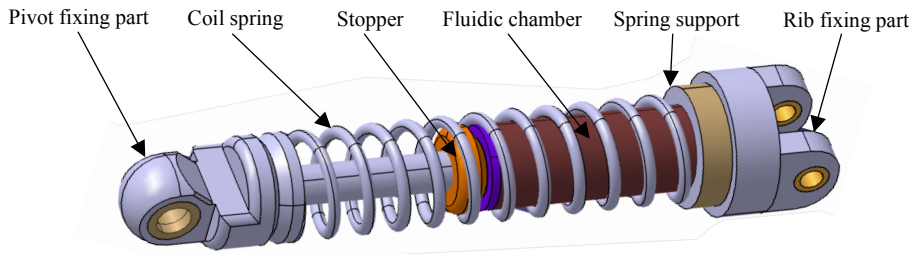
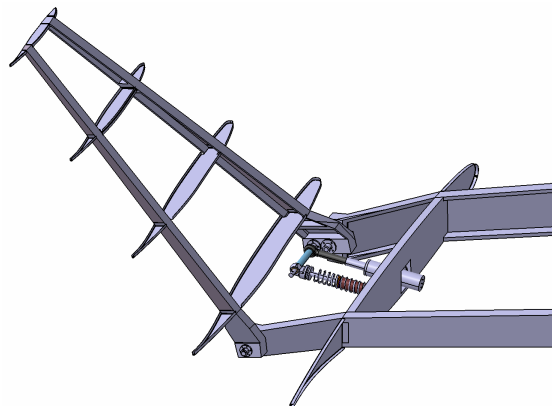


Figure 16: Morphing winglet damper design

This mechanism has been completely designed. The mechanism includes the pivot links in the spars, the pivot point which links the actuator to the mobile structure, the actuator connected to the fixed structure of the morphing winglet, as well as the damper. Through this mechanism, we noticed that we were able to vary it between the highest angles, from -90° to $+90^\circ$, which was our main objective. The lack of space to insert a mechanism varying the inclination of the winglet was a challenge that we were able to overcome. Indeed, this mechanism has only a small actuator travel for a large inclination of the winglet angle. In addition, it would be possible in the future to place multiple actuators on the pivot point shaft to add redundancy to the system, but it would add weight to the structure.

Figure 17: Morphing winglet assembly design at $+90^\circ$

4. MORPHING WINGLET STRUCTURAL ANALYSIS

In this paper, the entire structure of the morphing winglet has been studied through linear static analyses using HyperMesh. The geometry was imported from CATIA V5 into Hypermesh. Modeling a finite element structure needed to perform an accurate process of meshing. As a first step, we must carry out a geometrical simplification of the studied model with the aim to considerably reduce the computation time without damaging the general physics of the model. Then, the meshing phase of the model should take place, and makes it possible to geometrically model the structure of the morphing winglet by small finite elements called meshes. These elements will characterize the geometric behavior of the morphing winglet. Then, we will define the different materials and properties of the parts that make up the morphing winglet as well as the boundary conditions of our model. The morphing winglet will therefore be modeled in its operating environment. As a final step, some post-processing of the finite element modeling was done to ensure that the designed morphing winglet withstands the maximum load conditions.

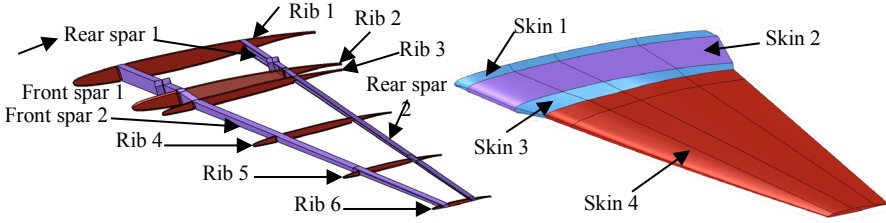


Figure 18: Initial morphing winglet geometry

In our structural model, the spars, ribs and skin are connected by numerous rivets. In order to simplify this model, we will not import the holes in the parts used to integrate the rivets. The fillets will be also removed to simplify the mesh of the model. In this paper, we will not consider as well the morphing winglet mechanism because we aim to study the internal structure only. As a result, we will mesh only the spars, the ribs and the skin portions. The different types of mesh elements for each structural components are described below :

Table 1: Element types for morphing winglet structural components

| Structural component | Element type |
|----------------------|-------------------------------|
| Skin | 2D quadrilateral |
| Ribs | 2D quadrilateral and triangle |
| Spars | 3D hexahedron |

Ribs and skin were designed with Catia’s surface and sheet metal tool. This is the reason why we used the mid-surface tool to simplify the mesh operation for 2D elements. The thickness and material of the components will be adjusted from the property window. By defining the density and the type of elements, we were able to design a mesh, meeting all the quality criteria, and which can be connected to the different elements. For the 3D mesh, we made a mesh by brick, which is a complex technique, but allows to precisely control the quality of the mesh that we want to have for our part. The spars being the main elements to support our loads, we decided to use a hexahedral mesh. This one generates a high quality mesh with a number of elements lower than a tetrahedral mesh and allow us to optimize the computation time.

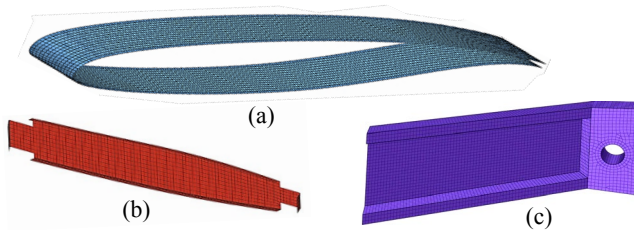


Figure 19: Structural component meshing: skin portion (a); rib (b); spar (c)

We ensured that all the surface and volume elements that we have meshed have their integrity at the level of their mesh. Indeed, the density of nodes and elements is identical. By performing a mesh of this kind, a very good quality of the general mesh for the analysis is obtained. The morphing winglet mesh assembly has 337,209 nodes and 397,856 elements. The quality of the mesh has been ensured, especially since we have 0.06% triangular elements for two-dimensional mesh elements and 1.2% pentagonal elements for three-dimensional mesh elements. Both figures are well below the acceptable 5% limit [6]. We have therefore carried

out a very good quality mesh and the number of elements is very well chosen for a low computation time. We finally get a fully meshed morphing winglet structure.

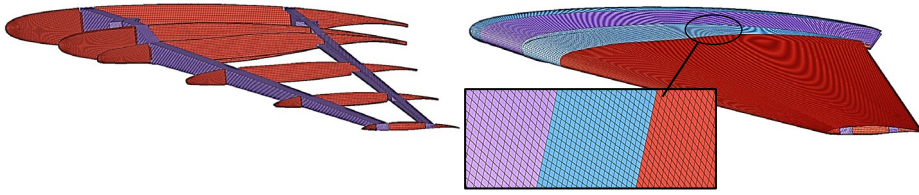


Figure 20: Fully meshed morphing winglet with mesh integrity

In order to quantify the quality of the mesh of the structural elements of the morphing winglet, various criteria must be analyzed. These criteria will allow us to measure the deviation of the elements using a grid compared to the ideal geometry. For 2D elements, we considered “Warpage” criterion, and the “Jacobian” criterion. The “Warpage” criterion is ideal at 0° and its maximum acceptable limit must be less than 10° for a 2D mesh. The “Jacobian” criterion is ideal for a value of 1 and its extremum must be greater than 0.6 to be defined as acceptable for a 2D mesh [6]. For 3D elements, we also used a criterion measuring the deviation of the elements with a grid compared to the ideal geometry. We will only consider the Jacobian criterion and the latter is ideal for a value of 1 and must be greater than 0.5 to be defined as acceptable for a 3D mesh [6]. We have therefore produced a very good quality mesh.

Table 2: Morphing winglet structural components mesh quality

| Structural component | Position | Jacobian criterion | Warpage criterion |
|----------------------|--------------------|--------------------|-------------------|
| Rib 1 | Front | 0.86 | 2.25 |
| | Middle | 0.82 | 1.06 |
| | Rear | 0.81 | 1.11 |
| Rib 2 | Front | 0.85 | 2.53 |
| | Middle | 0.81 | 0.61 |
| | Rear | 0.81 | 0.69 |
| Rib 3 | Front | 0.80 | 4.96 |
| | Middle | 0.82 | 0.65 |
| | Rear | 0.80 | 1.05 |
| Rib 4 | Front | 0.79 | 4.10 |
| | Middle | 0.84 | 0.46 |
| | Rear | 0.81 | 0.70 |
| Rib 5 | Front | 0.63 | 4.98 |
| | Middle | 0.79 | 0.31 |
| | Rear | 0.81 | 0.96 |
| Rib 6 | Front | 0.68 | 4.72 |
| | Middle | 0.74 | 0.52 |
| | Rear | 0.77 | 1.57 |
| Skin 1 | Wing connection | 0.91 | 1.77 |
| Skin 2 | Morphing portion | 0.60 | 2.39 |
| Skin 3 | Winglet connection | 0.74 | 4.98 |
| Skin 4 | Winglet | 0.90 | 3.09 |
| Front spar | 1 | 0.73 | |
| | 2 | 0.75 | |
| Rear spar | 1 | 0.61 | - |
| | 2 | 0.59 | |

We defined the characteristics of the holes in the spars allowing the rotation of the morphing winglet. Hexahedral elements allowed us to generate a finer mesh around the holes to accurately capture the constraint and displacement in this region. We used an RBE + BEAM approach to model the pivot connection. We connected the beam element to the holes with RBE elements transmitting only the degrees of freedom that were rigid. In the case of the pivot connection, the 3 translations and the bending rotations of the axis were transmitted but not the rotation around it. By using elements of type RBE2, the hole would not become oval. The pivot axis was modeled with a CBEAM element having the geometric and material properties of the shaft. This modeling allowed us to adequately represent our kinematics and to capture the load in the axis as well as the distribution in the spars.

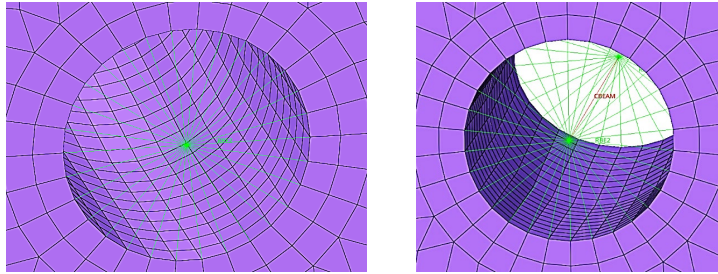


Figure 21: Pivot connection in spar

To link the skin portions, the ribs and the spars all together, we used rigid elements to act as rivets to connect these elements. We have chosen to use the CBEAM rigid connection element from HyperMesh. Indeed, this CBEAM element supports traction and compression, torsion, bending and shearing. Rigid elements are commonly used to represent rivets.

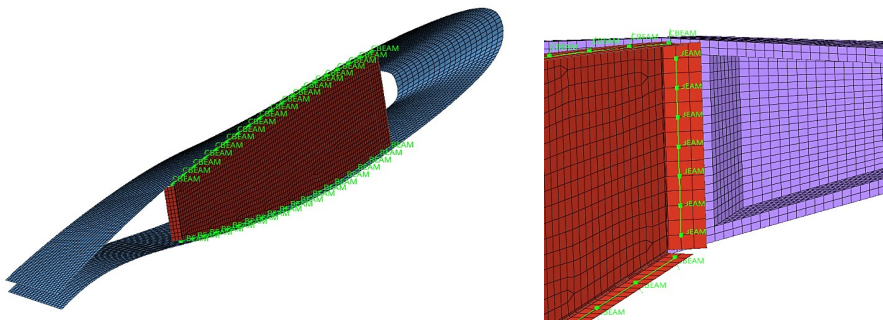


Figure 22: Rivet connections for the structural components of the morphing winglet

Before starting computation, we defined load cases and boundary conditions for our model. To represent the embedding of our structure, all degrees of freedom were fixed at the end of our spars. The main component of our study belongs to the aerodynamic loads applied to the adaptive winglet.

These aerodynamic loads are applied to the different parts of the skin as pressure forces, which will be transmitted to the internal structure due to rivet connections. In the aerodynamic studies that we carried out beforehand, the pressures values were obtained along the winglet.

We have defined pressure values varying from 0.18 MPa to 0.05 MPa. Simulations of the morphing winglet under extreme flight conditions were established. In this paper, we will simulate the wing up bending and the wing down bending by defining load factors of 4G and -2G, which are the limit values of load factor for the CRJ-700. We will also consider a 10G wing up bending load case.

The morphing winglet being meshed, it is essential to assign its materials. We have chosen to use for the spars and the ribs of the morphing winglet, an aluminum alloy 7075 T6. For the non-deformable skin, that is, we will use an aluminum alloy 7050 T651 with a 10 mm thickness.

The rivets will be made of steel 4140. Then, we propose a composite material which will constitute the morphing portion skin. A flexible honeycomb of 5 mm thickness was chosen for the sandwich center made of aluminum alloy 5056 F40. Next, we will apply a 2.5 mm layer of carbon in the direction perpendicular to the deformation of the morphing portion skin (90°) and then we add a 0.5 mm layer of EPDM elastomer in the direction of the deformation (0°).

In this configuration, we will precisely use the mechanical properties of the materials to model the morphing skin portion.

Table 3: Material mechanical properties and HyperMesh properties

| Structural component | Material | Young's Modulus [MPa] | Poisson Ratio | Shear Modulus [MPa] | Density [ton/mm ³] | Yield Strength [MPa] | Property |
|----------------------|---------------------|-----------------------|---------------|---------------------|--------------------------------|----------------------|------------------|
| Spars and Ribs | Aluminium 7075 T6 | 71 700 | 0.33 | 26 900 | 2.81 e-9 | 503 | PSOLID PSHELL |
| Skin | Aluminium 7050 T651 | 71 700 | 0.33 | 26 900 | 2.83 e-9 | 490 | PSHELL |
| Morphing skin | Al 5056 F40 | 1 276 | 0.35 | 310 / 117 | 0.0657 e-9 | 4.68 | PCOMP |
| | EPDM | 1.71 | 0.5 | 0.57 | 0.88 e-9 | 2.5 | PCOMP |
| | HexTow IM7 | 250 000 | 0.35 | 22 100 | 1.78 e-9 | 2 760 | PCOMP |
| Rivets | Steel 4140 | 205 000 | 0.29 | 80 000 | 7.85 e-9 | 1 050 | PBEAML |

We chose to study four load cases. A first load case was performed in which the morphing winglet was subjected only to maximum pressure forces, as well as to its weight. A second load case consisting of the morphing winglet subjected to maximum pressure forces and a load factor of 4G was realized. We analyzed a third load case where the morphing winglet was subjected to maximum pressure forces as well as a negative load factor of 2G.

A final load case was applied to the morphing winglet with maximum pressure forces and a load factor of 10G.

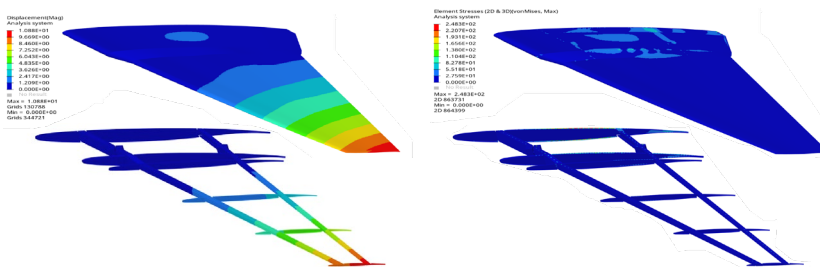


Figure 23: Distribution of displacement (a) and Von Mises stresses (b) along the morphing winglet (top) and internal structure (bottom) for load case 2

For each load case, we studied the maximum displacement and its location. The Von Mises and Tresca stress criteria were then obtained over the entire morphing winglet for different load cases (1, 2, 3 and 4). We have analyzed the maximum values of Von Mises stresses σ_{VM} and Tresca stresses σ_T for each component of the morphing winglet. Then, we compared the results of these stress analyses with the maximum allowable stresses using a 1.5 factor of safety [7].

Table 4: Von Mises and Tresca stresses results for the morphing winglet structural components

| Structural component | $\sigma_{VM,1}$ [MPa] | $\sigma_{T,1}$ [MPa] | $\sigma_{VM,2}$ [MPa] | $\sigma_{T,2}$ [MPa] | $\sigma_{VM,3}$ [MPa] | $\sigma_{T,3}$ [MPa] | $\sigma_{VM,4}$ [MPa] | $\sigma_{T,4}$ [MPa] | σ_{MAX} [MPa] |
|----------------------|-----------------------|----------------------|-----------------------|----------------------|-----------------------|----------------------|-----------------------|----------------------|----------------------|
| Spars | 146.1 | 158.4 | 154.9 | 165.2 | 145.8 | 159.2 | 294.3 | 309.6 | 335.3 |
| Ribs | 235.1 | 266.2 | 248.3 | 281.3 | 233.5 | 264.2 | 320.0 | 345.9 | 335.3 |
| Skin | 159.9 | 165.8 | 149.4 | 154.7 | 170.3 | 177.4 | 185.5 | 200.1 | 326.6 |

Based on the above results, for the maximum load factors of 4G and -2G that can be applied to the CRJ-700, the morphing winglet withstands very well. We have also highlighted the configuration corresponding to the fracture limit of the morphing winglet structure. In this study, it is the configuration for a load factor at 10G with the maximum pressure forces. It affected the ribs and more specifically the mid rib at the root of the morphing winglet. However, the spars still withstand this extreme load case.

We have verified that the structure withstands the most extreme load conditions by considering a safety factor of 1.5. Thanks to the mass calculation tool on HyperMesh, we were able to calculate the mass of the morphing winglet. The structure alone has a mass of 72.55 kg. Including the actuator and the damper, we would obtain a morphing winglet weighing less than 100 kg. This is a very encouraging result, as we could add approximately 600 kg for the actuation system alone [8].



Figure 24: Final morphing winglet design

5. CONCLUSIONS

The objective of this paper was to design a complete morphing winglet system allowing the CRJ-700 regional transport aircraft to optimize its aerodynamic performance in flight. The study was limited to the cruising phase under constant flight conditions at Mach number of 0.8 and at an altitude of 30,000 ft. We firstly found the winglet inclinations that provide the best aerodynamic performance for the CRJ-700 aircraft in its cruising phase. The results obtained demonstrated that when the airplane flies at a 0° angle of attack, the inclination of the winglet at 0° provides an increase in lift of 2.46% compared to the original inclination of the fixed winglet at $+73^\circ$. For this same angle of attack and winglet inclination, a 1.45% reduction in drag was achieved. The lift-to-drag ratio has therefore been increased by 3.95% for this configuration. However, when the aircraft is required to increase its angle of attack to 4° , the winglet inclination that provides the best aerodynamic performance remains the original $+73^\circ$ winglet inclination. We then designed a structure with a mechanism to vary the orientation of the morphing winglet between -90° and $+90^\circ$ inclination.

Then, we demonstrated that the designed morphing winglet structure would perfectly withstand the forces applied to it. In addition, we have designed a morphing winglet system

whose mass is low enough to keep aerodynamic benefits high enough, so that the mass of the morphing winglet would be less than 100 kg.

For future work, it will be interesting to analyze morphing wing work already done at our LARCASE laboratory its team. The LARCASE team, infrastructure and research methodologies are presented in [9]. Among the LARCASE publications, it is interesting to mention morphing horizontal tail and winglet aerodynamic research on the Cessna Citation X [10]-[11], on un-swept blended winglet [12], on several morphing wing configurations for the UAS-S4 and UAS-S45 [13]-[16], as well as on morphing wing-tip CRIAQ MDO 505 international project [17]-[21]. Structural research on morphing wing concepts for the UAS-S4 and UAS-S45 were presented in [22]-[23]. In the CRIAQ 7.1 and CRIAQ MDO 505 large-scale projects, morphing wing and morphing wing – tip (involving a wing and an aileron) were designed and further validated in the IAR-NRC wind tunnel [24]-[33]. In addition, other morphing wing and wing-tip models were developed at the LARCASE and validated using the Price-Paidoussis subsonic wind tunnel [34]-[37].

ACKNOWLEDGMENTS

The research described in this paper was performed on the Virtual Research Flight Simulator for Commercial Aircraft New Technologies Development (VRESIM), which was obtained with funds from the Canada Foundation for Innovation (CFI) and Ministère de l'Économie et d'Innovation. The VRESIM was developed by Aerospace companies CAE and Bombardier for research needs of the LARCASE team.

The authors would like to thank to the Natural Sciences and Engineering Research Council of Canada NSERC for the funds received within two research programs: the CREATE Uninhabited aircraft systems Training, Innovation and Leadership Initiative (UTILI) and the Canada Research Chair Tier 1 in Aircraft Modeling and Simulation Technologies.

REFERENCES

- [1] * * * ICAO. Aviation and the Environment, Montreal, Canada, 2016.
- [2] * * * IATA. Aviation & Climate Change Fact Sheet, April 2021.
- [3] M. Segui, F. Abel, R. Botez & A. Ceruti, Aerodynamic Modeling of an Aircraft using Open Foam: A High Fidelity Open Source Software – Application on the CRJ-700, *The Aeronautical Journal*, 1-22, 2021.
- [4] M. Segui, F. R. Abel, R. M. Botez, A. Ceruti, New Aerodynamic Studies of an Adaptive Winglet Application on the Regional Jet CRJ700, *Biomimetics*, Special Issue: Aircraft Morphing Systems 2.0, Vol. 6(4), 54, pp. 1-28, 2021.
- [5] M. Arena, F. Amoroso, R. Pecora & S. Ameduri, Electro-Actuation System Strategy for a Morphing Flap, *Aerospace*, 6(1), 1. URL: <https://doi.org/10.3390/aerospace6010001>, 2018.
- [6] N. S. Gokhale, S. S. Deshpande, S. V. Bedekar, A. N. Thite, *Practical Finite Element Analysis* (1st éd.), Maharashtra, Ind : Finite To Infinite, 2021.
- [7] * * * Code of Federal Regulations, Factor of safety, Norm 14 CFR § 25.303, 2002.
- [8] F. R. Abel, *Aerodynamic Improvement of the Bombardier CRJ700 using morphing technologies application on winglets*, Università di Bologna, Italy, 2019.
- [9] R. M. Botez, Morphing Wing, UAV and Aircraft Multidisciplinary Studies at the Laboratory of Applied Research in Active Controls, Avionics and AeroServoElasticity LARCASE, *AerospaceLab Journal*, ONERA, Vol. 14(2), pp. 1-14, <https://hal.archives-ouvertes.fr/hal-01935171/>, 2018.
- [10] M. Segui, S. Bezin, R. M. Botez, Cessna Citation X Performance Improvement by an Adaptive Winglet during the Cruise Flight, *International Journal of Mechanical, Industrial and Aerospace Sciences*, vol. 11(4), 2018.
- [11] M. Segui, M. Mantilla, R. M. Botez, Design and Validation of an Aerodynamic Model of the Cessna Citation X Horizontal Stabilizer Using both OpenVSP and Digital Datcom, *International Journal of Mechanical, Industrial and Aerospace Sciences*, vol. 11(1), 2018.

- [12] H. Aubeelack, R. M. Botez, Simulation Study of the Aerodynamic Force Distributions on the UAS-S45 Baalam Wing with an Upswept Blended Winglet, *INCAS Bulletin*, Vol. **11**(1), pp. 21-38, <https://doi.org/10.13111/2066-8201.2019.11.1.2>, 2019.
- [13] O. Sugar Gabor, A. Koreanschi, R. M. Botez, A New Non-Linear Vortex Lattice Method: Applications to Wing Aerodynamic Optimizations, *Chinese Aeronautical Journal*, Vol. **29**(5), pp. 1178-1195, 2016.
- [14] O. Sugar Gabor, A. Koreanschi, R. M. Botez, Analysis of UAS-S4 Ehécatl Aerodynamic Performance Improvement using Several Configurations of a Morphing Wing Technology, *The Aeronautical Journal*, Vol. **120**(1231), pp. 1337-1364, 2016.
- [15] O. Sugar Gabor, A. Simon, A. Koreanschi, R. M. Botez, Aerodynamic Performance Improvement of the UAS-S4 Ehécatl Morphing Airfoil using Novel Optimization Techniques, *Proceedings of the Institution of Mechanical Engineers, Part G: Journal of Aerospace Engineering*, Vol. **230**(7), pp. 1164-1180, 2016.
- [16] O. Sugar Gabor, A. Simon, A. Koreanschi, R. M. Botez, Improving the UAS-S4 Ehécatl Airfoil High Angle of Attack Performance Characteristics using a Morphing Wing Approach, *Proceedings of the Institution of Mechanical Engineers, Part G: Journal of Aerospace Engineering*, Vol. **23**(2), pp. 118-131, 2016.
- [17] A. Koreanschi, O. Sugar Gabor, J. Acotto, G. Brianchon, G. Portier, R. M. Botez, M. Mamou, Y. Mébarki, Optimization and Design of an Aircraft's Morphing Wing-Tip Demonstrator for Drag Reduction at Low Speeds, Part I - Aerodynamic Optimization using Genetic, Bee Colony and Gradient Descent Algorithms, *Chinese Journal of Aeronautics*, Vol. **30**(1), pp. 149-163, 2017.
- [18] A. Koreanschi, O. Sugar Gabor, J. Acotto, G. Brianchon, G. Portier, R. M. Botez, M. Mamou, Y. Mébarki, Optimization and Design of an Aircraft's Morphing Wing-Tip Demonstrator for Drag Reduction at Low Speeds, Part II - Experimental Validation using Infra-Red Transition Measurement from Wind Tunnel Tests, *Chinese Journal of Aeronautics*, Vol. **30**(1), pp. 164-174, 2017.
- [19] A. Koreanschi, O. Sugar Gabor, R. M. Botez, Drag Optimization of a Wing Equipped with a Morphing Upper Surface, *The Aeronautical Journal*, Vol. **120**(1225), pp. 473-493, 2016.
- [20] A. Koreanschi, M. B. Henia, O. Guillemette, F. Michaud, Y. Tondji, O. Sugar Gabor, R. M. Botez, M. Flores Salinas, Flutter Analysis of a Morphing Wing Technology Demonstrator: Numerical Simulation and Wind Tunnel Testing, National Institute for Aerospace Research "Elie Carafoli" *INCAS Bulletin*, Vol. **8**(1), pp. 99-124, <http://dx.doi.org/10.13111/2066-8201.2016.8.1.10>, 2016.
- [21] R. M. Botez, A. Koreanschi, O. Sugar-Gabor, I. Tondji, M. Guezguez, M. J. Tchatchueng Kammegne, L. T. Grigorie, D. Sandu, Y. Mebarki, M. Mamou, F. Amoroso, R. Pecora, L. Lecce, G. Amendola, I. Dimino, A. Concilio, Numerical and Experimental Transition Results Evaluation for a Morphing Wing and Aileron System, *The Aeronautical Journal, Smart Aircraft Issue*, Vol. **122**(1251), pp. 747-784, 2018.
- [22] M. Elelwi, T. Calvet, R. M. Botez, T. M. Dao, Wing Components Allocation for a Morphing Variable Span Tapered Wing using Finite Elements Method and Topology Optimization – Application to UAS-S4, *The Aeronautical Journal*, pp. 1-24, 2021.
- [23] M. Elelwi, M. A. Kuitche, R. M. Botez, T. M. Dao, Comparison and Analyses of a Variable Span Morphing of Tapered Wing with a Varying Sweep Angle, *The Aeronautical Journal*, Vol. **124**(1278), pp. 1146-1169, 2020.
- [24] L. T. Grigorie, R. M. Botez, A. V. Popov, M. Mamou, Y. Mébarki, A Hybrid Fuzzy Logic Proportional-Integral-Derivative and Conventional On-Off Controller for Morphing Wing Actuation using Shape Memory Alloy, Part 1: Morphing System Mechanisms and Controller Architecture Design, *The Aeronautical Journal*, Vol. **116**(1179), pp. 433-449, 2012.
- [25] L. T. Grigorie, R. M. Botez, A. V. Popov, M. Mamou, Y. Mébarki, A Hybrid Fuzzy Logic Proportional-Integral-Derivative and Conventional On-Off Controller for Morphing Wing Actuation using Shape Memory Alloy, Part 2: Controller Implementation and Validation, *The Aeronautical Journal*, Vol. **116**(1179), pp. 451-465, 2012.
- [26] L. T. Grigorie, R. M. Botez, A.-V. Popov, How the Airfoil Shape of a Morphing Wing is Actuated and Controlled in a Smart Way, *The Journal of Aircraft Engineering*, American Society of Civil Engineers ASCE Edition, Vol. **28**(1), 2015.
- [27] M. J. Tchatchueng Kammegne, L. T. Grigorie, R. M. Botez, A. Koreanschi, Design and Wind Tunnel Experimental Validation of a Controlled New Rotary Actuation System for a Morphing Wing Application, *Proceedings of the Institution of Mechanical Engineers, Part G: Journal of Aerospace Engineering*, Vol. **230**(1), pp. 132-145, 2015.
- [28] M. J. Tchatchueng Kammegne, L. T. Grigorie, R. M. Botez, Design, Numerical Simulation and Experimental Testing of a Controlled Electrical Actuation System in a Real Aircraft Morphing Wing Model, *The Aeronautical Journal*, Vol. **119**(1219), pp. 1047-1072, 2015.
- [29] M. J. Tchatchueng Kammegne, R. M. Botez, L. T. Grigorie, M. Mamou, Y. Mébarki, Proportional Fuzzy Feed-Forward Architecture Control Validation by Wind Tunnel Tests of a Morphing Wing, *Chinese Aeronautical*

- Journal*, Vol. **30**(2), pp. 561-576, 2017.
- [30] M. J. Tchatchueng Kammegne, Y. Tondji, R. M. Botez, L. T. Grigorie, M. Mamou, Y. Mébarki, New Control Methodology for a Morphing Wing Demonstrator, *Proceedings of the Institute of Mechanical Engineers IMechE, Part G: Journal of Aerospace*, Vol. **232**(8), pp. 1479-1494, 2017.
- [31] S. Khan, T. L. Grigorie, R. M. Botez, M. Mamou, Y. Mébarki, Fuzzy Logic based Control for a Morphing Wing-Tip Actuation System: Design, Numerical Simulation and Wind Tunnel Experimental Testing, Manuscript ID: biomimetics-576000, *Biomimetics*, Vol. **4**(4), 65, Special Issue: Morphing Aircraft Systems, 2019.
- [32] S. Khan, T. L. Grigorie, R. M. Botez, M. Mamou, Y. Mébarki, Novel Morphing Wing Actuator Control based Particle Swarm Optimization, *The Aeronautical Journal*, Vol. **124**(1271), pp. 55-75, 2019.
- [33] M. J. Tchatchueng Kammegne, L. T. Grigorie, R. M. Botez, A. Koreanschi, Design and Wind Tunnel Experimental Validation of a Controlled New Rotary Actuation System for a Morphing Wing Application, *Proceedings of the Institution of Mechanical Engineers, Part G: Journal of Aerospace Engineering*, Vol. **230**(1), pp. 132-145, 2015.
- [34] D. Communier, R. Botez, T. Wong, Design and Validation of a New Morphing Camber System by Testing in the Price-Paidoussis Subsonic Wind Tunnel, *Aerospace, MDPI Edition, Special Issue: Design and Analysis of Wind-Tunnel Models and Fluidic Measurements*, Vol. **7**(23), pp. 1-22, 2020.
- [35] D. Communier, R. M. Botez, M. Kuitche, Experimental Validation of a New Morphing Trailing Edge System using Price-Paidoussis Wind Tunnel Tests, *Chinese Journal of Aeronautics*, Vol. **32**(6), pp. 1353-1366, 2019.
- [36] A. Koreanschi, O. Sugar Gabor, R. M. Botez, Numerical and Experimental Validation of a Morphed Wing Geometry Using Price-Paidoussis Wind Tunnel Testing, *AIAA Aviation 2015*, 33rd AIAA Applied Aerodynamics Conference, Dallas, TX, USA, June 22-26, 2015.
- [37] D. Communier, M. Salinas Flores, O. Carranza Moyao, R. M. Botez, Aero-Structural Modeling of a Wing using CATIA V5 and XFLR5 Software and Experimental Validation using the Price-Paidoussis Wind Tunnel, *AIAA Aviation 2015*, AIAA Atmospheric Flight Mechanics Conference, Dallas, TX, USA, June 22-26, 2015.